

Wall temperature effects on aerodynamic heating mechanisms in shock wave turbulent boundary layer interaction

Zhenyuan Tang, Haonan Xu, Xueying Li & Jing Ren

Tsinghua University, Beijing, 100084, China

Abstract

Due to the wall temperature difference between wind tunnel experiments and flight environment, the wall temperature effects on shock wave turbulent boundary layer interaction (STBLI) are worth investigating. Based on the verified DNS method, a 30 degree compression ramp is used to generate STBLI for Ma of 5 and wall to recovery temperature ratio ranging from 0.2 to 1.0. The results indicate that the separation zone decreases for cold wall conditions and quantitatively validate the wall-temperature-corrected interaction scaling theory in recent literature. The heat transfer results show that the wall temperature greatly influence the heat flux distribution and peak values in STBLI. A distinct two-stage heat flux increase is observed for the hot wall, which corresponds to the expanded separation bubble. The local decrease of the recovery temperature is observed after the shock, which causes the negative heat flux minimum for near "adiabatic" wall conditions and can be attributed to the acceleration of the near-wall supersonic fluid in turning process. Overall, the decrease of wall temperature leads to the decrease of the peak heat flux enhancement and the fundamental mechanisms is the near-wall turbulent aerodynamic heat dissipation variation with wall temperatures.

Keywords: aerodynamic heating, shock wave turbulent boundary layer interaction, wall cooling, direct numerical simulation.

1. Introduction

Shock wave turbulent boundary layer interaction (STBLI) widely exists in high speed flight, which raises serious aerodynamic heating problems and must be considered in aircraft designs[1]. Recently, wall temperature effects on shock wave turbulent boundary layer interaction has become a new research hotspot. On one hand, the wall temperature conditions in ground wind tunnel tests are far different from that in actual flight environments[2] and therefore people want to know more about the difference between ground test data and flight data. On the other, wall cooling is a promising method in controlling high-speed compressible flows[3].

In compressible flows at high Ma, wall temperature changes will cause a strong coupling changes of the velocity and the temperature field. Previous studies have revealed the wall temperature effects on the flow structures of STBLI in detail. As early as in the 1970s, experimental studies by Spaid et al.[4] and Back et al.[5] found that wall cooling can weaken the separation induced by shock waves. In recent years, high-fidelity numerical simulations[6] have also confirmed the conclusion and extended it to hypersonic conditions[7]. Quantitatively, Spaid et al.[4] observed a linear relationship between separation lengths and wall temperatures based on experimental data while Zhu et al.[2] derived a semi-theoretical correlation which pointed out that the separation length is proportional to the 0.85th power of the wall temperature. At present, the consensus has been reached on the mechanisms of the wall temperature effects on the shock induced separation: (1) the cooling wall reduces the fluid viscosity, which makes the velocity profile fuller near the wall and stronger to resist separation; (2) the cooling wall lowers the sound speed line leading to smaller subsonic zone, which inhibits pressure from travelling upstream and hence reduces the separation area. Another important quantitative parameter is the interaction length which has been theoretically analyzed and correlated to the dimensionless shock strength by Souverein et al.[9]. Later, the theory was corrected for nonadiabatic wall conditions[10] and the corrected correlation has been verified by some recent research[7][8]. These studies also indicated that the interaction length decreases as the wall temperature decreases.

Wall temperatures also have significant impacts on the turbulent structures and fluctuation in STBLI. Wall cooling make turbulent kinetic energy decrease and move further away from the wall[12]. Tong et al.[11] pointed out that the cold wall strengthened the coherence in streamwise direction and the small scale vortices are significantly enhanced. Zhu et al.[12] pointed out that at lower wall temperatures, the evolution of near wall streamwise vortices into complex three-dimensional structures is decelerated and the scale of the downstream counter-rotating vortices decreases. In addition, wall temperatures also affect the low-frequency fluctuation which is an important topic in STBLI and has been investigated extensively. Experimental measurements by Jaunet et al.[10] showed that low-frequency oscillations are more obvious for the hot wall and the numerical results of Tong et al.[11] also indicated that the intermittent region of shock oscillation decreases for cold wall, causing the low-frequency peaks in the spectrum to shift towards higher frequency. In conclusion, cold walls effectively suppress low-frequency oscillations in STBLI.

However, due to the strong coupling of flow and heat transfer, the wall temperature effects on aerodynamic heating are more complex and the research is limited. The numerical results of Bernardini et al.[6] indicated that the Stanton number shows the complex spatial variation in interaction area, which strongly depends on the wall to recovery temperature ratios. They explained that the cooling wall reduces the separation scale and therefore increases the temperature gradient, which makes St peak is amplified. They further related the peak heat flux to the pressure fluctuation amplification.

In recent years, research on the wall temperature effects has been gradually conducted, which adds some new insight to previous STBLI studies which mainly focused on adiabatic wall conditions. However, the recent studies mainly provided temperature effects on flow field but not on aerodynamic heating. Therefore, the wall temperature effects and influence mechanisms on aerodynamic heating still need to be further studied. Based on direct numerical simulation (DNS), this study verifies the wall temperature effects on interaction length proposed by Jaunet et al.[10], further investigates the wall temperature effects on the aerodynamic heat generation in high-speed flows and reveals the mechanisms of the wall heat flux changes for different wall temperature conditions.

2. DNS Method and Validation

2.1 Computational Domain and Numerical Methods

Four compression ramp flows with the same angle of 30 degree for the same Ma of 5 but different wall temperatures are used to investigate the STBLI as listed in Table 1 and the computational domain covered by the grid is shown in Fig. 1. Corresponding 2D auxiliary simulations are conducted to provide the inlet laminar profiles for 3D turbulent simulation. The origin of the coordinate system is set at the corner vertex. L_{x1} is the streamwise length for turbulent boundary layer and L_{x2} is the ramp length, L_y is the wall-normal length, L_z is the spanwise length. The specific values of these lengths for different wall temperature cases are listed in Table 1. The lengths of boundary layer development, L_{x1} , have been selected to match the Re_θ of the turbulent boundary layer for different wall temperature conditions, which will be discussed later. L_{x2} have been set as 60 mm for all cases. The spanwise two point correlations of the fluctuating velocity proved that the domain spanwise scales are sufficient to solve the largest scale vortices as shown in Fig. 2.

The governing equations are Navier-Stokes equations in curvilinear coordinate system[13] and the boundary conditions are similar to these of the hypersonic boundary layer DNS by Duan et al.[14] with freestream Ma of 5. The compressible laminar boundary layer profiles for corresponding wall temperatures are used at the inlets to reduce computational cost, which is obtained from 2D simulations. Forced transition of boundary layers is realized by introducing blowing and suction disturbance[15] to get turbulent boundary layers, which is set 20 mm behind the inlets on the wall.

The governing equations are discretized on the structural grid by the finite difference method. The first layer grid heights y^+ all are around 0.35 and the maximum y^+ downstream of the corner are controlled to around 0.6 as listed in Table 2. The maximum grid number reaches 4.16×10⁸ of case T02. As the wall temperature increases, the wall viscous scale increases and hence the total grid

Wall temperature effects on aerodynamic heating mechanisms in STBLI

number can be reduced to achieve the same accuracy. The grids are proved sufficient to solve turbulence, which will be discussed carefully in next subsection. Convection terms are solved by a hybrid scheme which is composed of a 7-order low dissipation upwind scheme in smooth region, a 7-order WENO scheme in non-smooth region and a 5-order WENO scheme in extremely non-smooth region. Time stepping is conducted by the 3rd-order Runge-Kutta method. To ensure the numerical stability, the time steps have been carefully selected based on Courant number and pilot calculation. The computations were performed on the open source code OpenCFD-SC which has been widely validated by the development team[16] -[18].

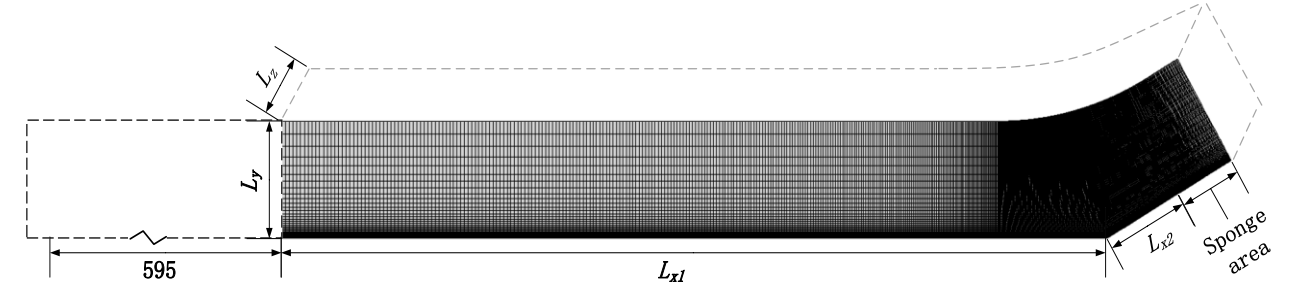


Figure 1 - Computational domain and grid of STBLI. Auxiliary 2D simulations are conducted to provide laminar profiles in the inlet of the 3D simulations of STBLI and the 3D computational domain is the area covered by grids.

Case	T_w/T_r	Ma Re/mm		$L_{x1} \times L_y \times L_z$ [mm]	$L_{x1} \times L_y \times L_z / \delta$		
T02	0.2	5	7980	$260\times60\times15$	$34.8 \times 7.8 \times 2.0$		
T05	0.5	5	7980	$460 \times 60 \times 30$	$43.4 \times 5.7 \times 2.8$		
T08	0.8	5	7980	$460 \times 60 \times 30$	$50.0 \times 6.5 \times 3.3$		
T10	1.0	5	7980	$460\times60\times30$	$52.9 \times 6.9 \times 3.5$		

Table 1 Main condition parameters and computational domain sizes

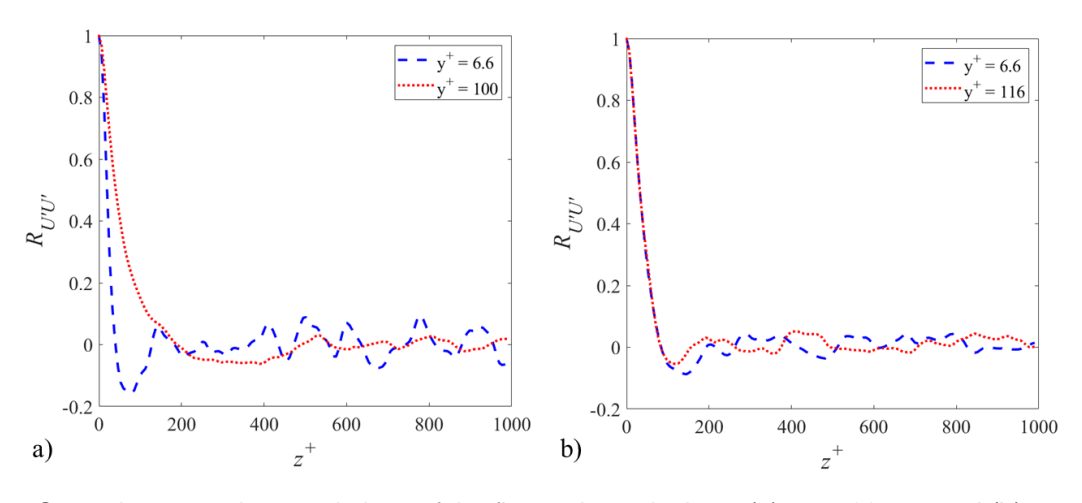


Fig. 2 Spanwise two point correlations of the fluctuating velocity at (a) x = -60 mm and (b) x = 0 mm.

The flows are steady on average and hence sampling statistics are conducted. The sampling time duration listed in Table 2 has been checked to ensure time convergence. Particularly, this study statistically calculated all items in the heat transport equation, Eq. (1), during the calculation process to explore the mechanisms of temperature effects on aerodynamic heat generation and transport in STBLI. Note that \bar{x} means Reynolds average while \tilde{x} means Favre average, x' and x'' mean the corresponding fluctuation.

							,				
_	Case	y ⁺ @ref	y ⁺ @max	N_x	N_z	N_y	N_{total}	Time step $U\Delta t/L_{ref}$	Sampling time UT/L_{ref}		
	T02	0.41	0.65	4400	420	225	4.16×10^{8}	0.0025	500		
	T05	0.33	0.59	2660	300	204	1.63×10^{8}	0.0060	900		
	T08	0.34	0.63	2660	200	180	0.96×10^{8}	0.0125	1200		
	T10	0.31	0.6	2660	160	172	0.73×10^{8}	0.0150	1200		

Table 2 Computational grid and time step setups for the DNS of STBLI for different wall temperature conditions. (Note: Reference location is at x = -60 mm. $L_{ref} = 1$ mm)

$$\frac{\partial \bar{\rho} \widetilde{u_j} \widetilde{h}}{\partial x_j} + \frac{\partial \bar{\rho} u_j^{\prime \prime} h^{\prime \prime}}{\partial x_j} + \frac{\partial}{\partial x_j} \left(-\lambda \frac{\partial \bar{\tau}}{\partial x_j} \right) = \bar{u_j} \frac{\partial \bar{p}}{\partial x_j} + \bar{u_j}^{\prime} \frac{\partial p^{\prime}}{\partial x_j} + 2\mu \overline{S_{ij}^d} \, \overline{S_{ij}^d} + 2\mu \overline{S_{ij}^{d^{\prime}} S_{ij}^{d^{\prime}}}$$
(1)

2.2 Grid with Independence Test

Grid quality largely influences DNS quality and the near-wall grid largely influences the wall gradients like wall frictions and wall heat fluxes. Taking case T05 and T08 as examples, two grid independence tests were conducted with 8 sets of grids as shown in Table 3. For case T05, the total grid number varies from $1.25 \times 10^8 \sim 1.81 \times 10^8$ and for case T08 varies in a larger range from $9 \times 10^6 \sim 1.44 \times 10^8$. The tests mainly focus on the independence of normal grids, which is important for the present research purpose, i.e. calculation of wall shear stresses and wall heat fluxes. The wall normal grid Reynolds number Re_{Δ_n} is also given to estimate the grid quality in the table, which is suggested around 10 generally and can be relaxed to even 40 for low-dissipation numerical schemes [19]. The normal growth rates of all cases are kept close while the wall-normal grid number varies.

Table 3 Grid setup for the independence test of case T05 and case T08. (The cases are named by the basic case of different wall temperature conditions.)

Case	T05M1	T05M2	T05M3	T05M4
Grid number / million	125	144	163	181
y+@ref	1.31	0.66	0.33	0.16
y+@max	2.08	1.15	0.59	0.30
$Re_{\Delta_{\mathrm{n}}} = \rho_{w} U_{e} \Delta_{\mathrm{n}} / \mu_{w}$	28	14	7	4
z+@ref	6.6	6.6	6.6	6.6
Normal growth rate	1.0292	1.0293	1.0293	1.0295

Table 3 (Continued)

Case	T08M1	T08M2	T08M3	T08M4
Grid number / million	9	50	96	144
y+@ref	2.03	0.93	0.34	0.38
y+@max	3.51	1.80	0.63	0.76
$Re_{\Delta_{ m n}} = ho_w U_e \Delta_{ m n}/\mu_w$	84	35	13	14
z+@ref	13.5	7.0	5.7	3.8
Normal growth rate	1.038	1.028	1.027	1.029

The separation lengths around the corner are used to determine the grid independency as shown in Fig. 3. The results show that the separation length decreases as the total grid number increases. Case T05M3 and T08M3 reach grid independency respectively.

The wall pressure and skin friction distribution are further investigated to confirm the grid independency and the results are given in Fig. 4. It can be seen that the wall pressure distribution is

insensitive to the grid, which further indicates that the interaction length is also insensitive to the grid. For skin friction coefficient, the upstream area reaches grid convergence while the grid have great influence on the wall friction downstream of the corner. Case T05M3 shows good grid convergence downstream of STBLI as shown in Fig. 4(b). Case T08M3 basically reaches grid independence with acceptable error. Above all, the grid-independent case T05M3 and T08M3 will be used to analyze wall temperature effects on aerodynamic heating mechanisms.

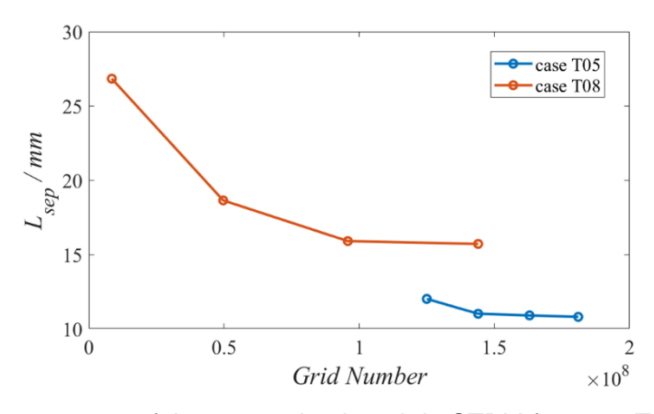


Fig. 3 Grid convergence of the separation length in STBLI for case T05 and case T08.

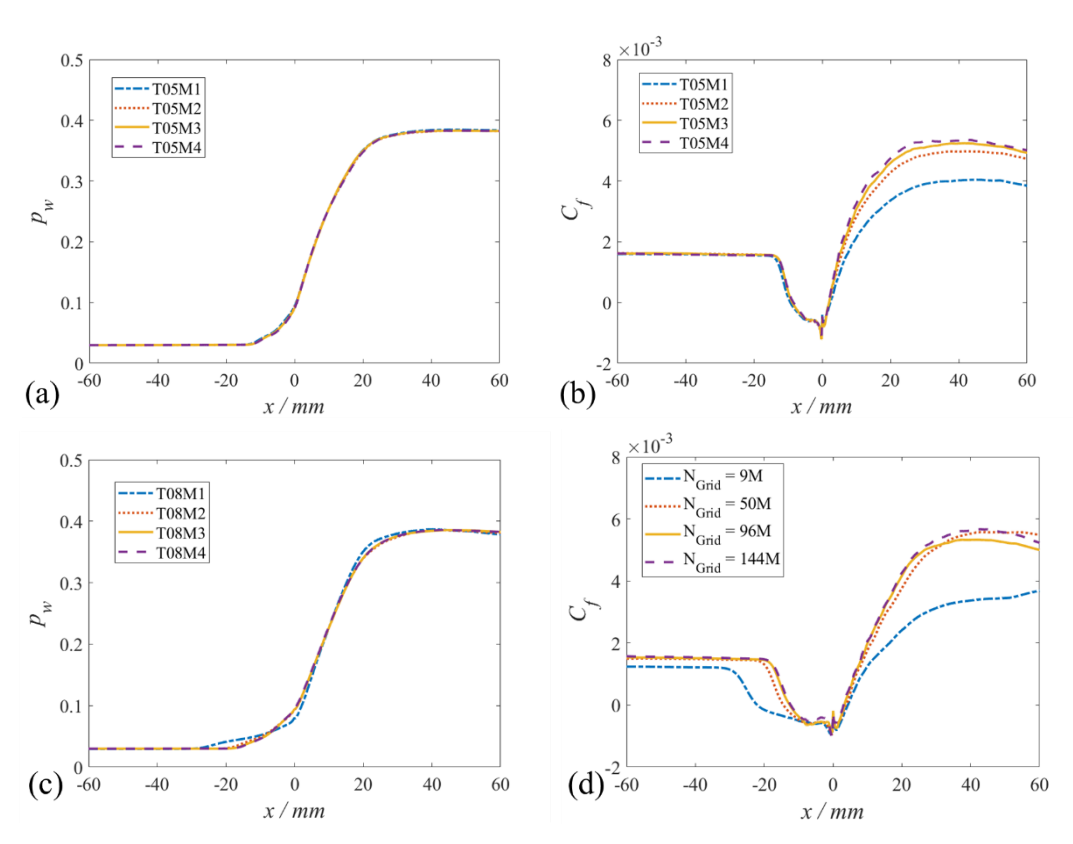


Fig. 4 (a)(c) Wall pressure and (b)(d) friction coefficient distribution computed by different grids for case T05 and case T08.

2.3 Characteristics of Incoming Boundary Layer

The boundary layer characteristics at the reference station (x=-60 mm) are provided in Table 4, including boundary layer thickness, profile factors, some common-use Reynolds numbers, skin friction coefficients and Stanton numbers. The nominal thickness δ will be used to nondimensionalize length quantity and the displacement thickness δ^* will be used to predict the interaction length. The profile factor H increases as the wall temperature increases, which indicating that the velocity profile becomes more defective for higher wall temperature conditions. Re_{θ} for all cases are kept close

around 4,000 to weaken the effect of incoming turbulent boundary layer states on the STBLI so that the wall temperature effects can be investigated more dependently. Re_{τ} , which is defined as $\rho_w u_{\tau} \delta/\mu_w$, varies between different temperature cases because the fluid properties on the wall strongly depends on the wall temperature. Recently a more appropriate friction Reynolds number Re_{τ}^* was proposed by Trettel et al.[21], which is based on mainstream fluid properties and defined as $\rho_{\infty}u_{\tau}\delta/\mu_{\infty}$. The result shows that Re_{τ}^* of different cases are also close as listed in Table 4. C_f and St results indicate that cold walls increase the skin friction and heat transfer of the incoming turbulent boundary layers. The Reynolds analog factors are around 1.1 and slightly increase with wall temperature decreasing, which is consistent with the study of Duan et al.[14].

			•					• •	•	
•	Case	δ/mm	$\delta^*/{ m mm}$	$H = \delta^*/\theta$	$Re_{ heta}$	$Re_{ au}$	$Re_{ au}^*$	Cf	St	2St/Cf
	T02	7.7	2.4	5.2	3600	1760	1960	2.06×10^{-3}	1.21×10^{-3}	1.17
	T05	10.6	3.3	5.9	4500	700	2400	1.61×10^{-3}	0.93×10^{-3}	1.16
	T08	9.2	4.0	8.9	3600	350	2030	1.53×10-3	0.83×10^{-3}	1.08
	T10	8.7	4.5	11.4	3200	250	1840	1.37×10^{-3}	-	-

Table 4 Characteristic parameters of the undisturbed turbulent boundary layers at reference position.

Velocity profiles and temperature profiles of the undisturbed turbulent boundary layer at the reference station are further validated by comparing with some previous theories. The van Driest transformation[20] of velocity profiles are provided in Fig. 5(a) with the wall law of incompressible boundary layers. The results show that the profile of adiabatic wall collapses well with the wall law of incompressible turbulent boundary layers. All velocity profiles show notable linear and logarithmic region but with some difference in detail. The linear region in the viscous sublayer is small for cold walls, especially for case T02, which can be explained by the decreased molecular viscosity and small viscosity-dominated region. In addition, the wake layer is higher for colder wall conditions. After considering the influence of wall temperatures, the Trettel-Larsson transformation velocity profiles [21]are calculated and show better agreement with the wall law for all wall temperature cases as shown in Fig. 5(b), except for the slight deviation of case T02 wake layer. The deviation is caused by the limitation of the present computational domain of case T02, leading to the influence of the inlet Mach wave which goes through the profiles at the reference station (x=-60 mm) as clearly shown in Fig. 7. Fortunately, the inlet Mach wave does not influence STBLI around the corner.

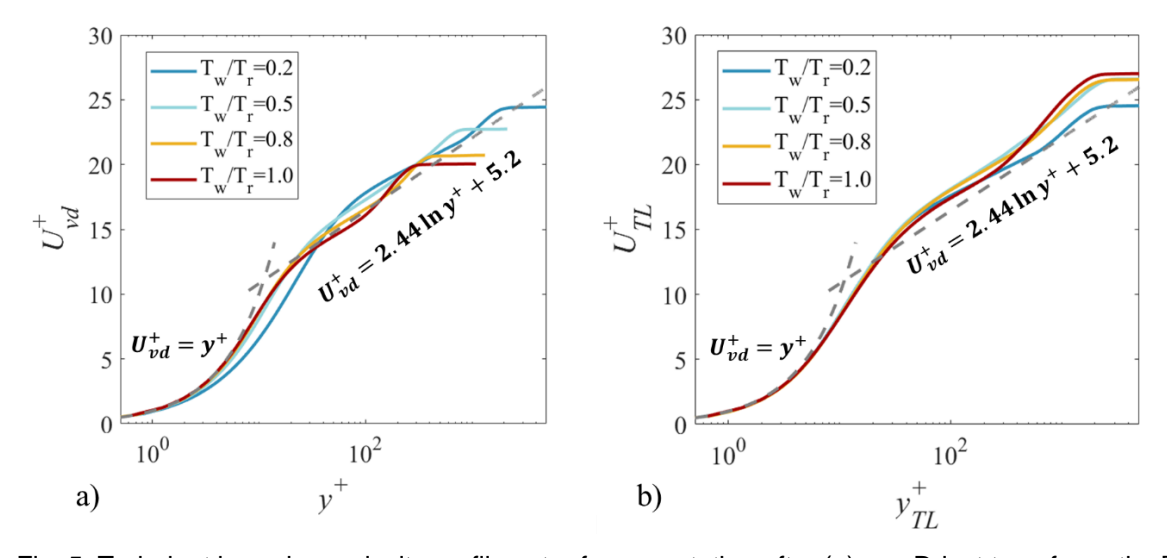


Fig. 5 Turbulent boundary velocity profiles at reference station after (a) van Driest transformation[20] and (b) Trettel-Larsson transformation[21].

The velocity-temperature relationship is also important in compressible boundary layer. The DNS results are compared with Walz relationship [22]as shown in Fig. 6(a), showing that the adiabatic case collapse with Walz theory but cold-wall cases deviate from Walz theory. The deviation can be attributed to the failure of the strong Reynold analog in non-adiabatic cases. Recently, Zhang et al. [23]proposed a generalized relation which considers wall heat transfer effects. The results given in Fig. 6(b) shown that the corrected prediction of Zhang's relation are in great agreement with the present DNSs.

In conclusion, the results of turbulent boundary layer proved the reliability of the wall temperature effects on the calculation results.

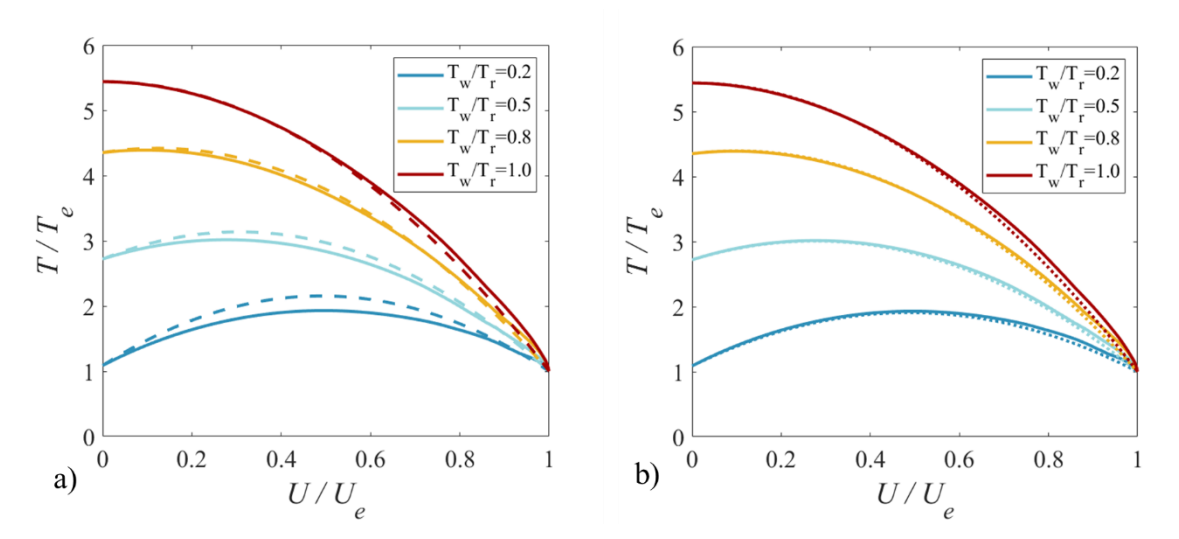


Fig. 6 Velocity and temperature relations of incoming turbulent boundary velocity profile at reference station (solid lines) compared with (a) Walz relation theory (dash lines)[22]and (b) Zhang relation theory (dash lines).

3. Wall Temperature Effects on Flow Structures in STBLI

The instantaneous flow fields of the whole computational domains are shown in Fig. 7. The results indicate that the boundary layer transition is advanced with the decrease of wall temperature and for this reason the streamwise length of case T02 domain has been reduced to control the development degree of turbulent boundary layer and hence control the Re_{θ} . In upstream undisturbed turbulent boundary layer, the coherent structures at the edge of the boundary layer induce small shocklets in the mainstream, indicating that the fluctuating Mach number exceed 1 at the edge of the boundary layer. In interaction region, the separation zones shrink as the wall temperature decreases. The turbulent coherent structures cause the fluctuating of shock waves when passing through the shock waves and the fluctuation decreases with the decrease of the wall temperature.

From the x-z plane, the instantaneous flow fields show some interesting structures and the wall temperature effect are significant as shown in the slices of $y^+=10$ in Fig. 8. In upstream undisturbed turbulent boundary layer, there exist typical velocity streaks and the spacing between the adjacent streaks all are about $200~\delta_{\nu}$ for all wall temperature cases. As the wall temperature decrease, the streaks become more straight and well-organized. In interaction region, there exist irregular and turbulent separation zones. Interestingly, the separation zones are not continuous in spanwise direction but show some large-scale spanwise periodicity, for example there exist 2 separation bubbles in spanwise direction for case T10. It can be seen more clearly that the separation zones decrease as the wall temperature decreases. Downstream of the reattachment lines, some large-scale streaks appear, which were explained by the Gortler instability in previous literature[24]-[26]. As the wall temperature decreases, the large-scale streaks also become more straight.

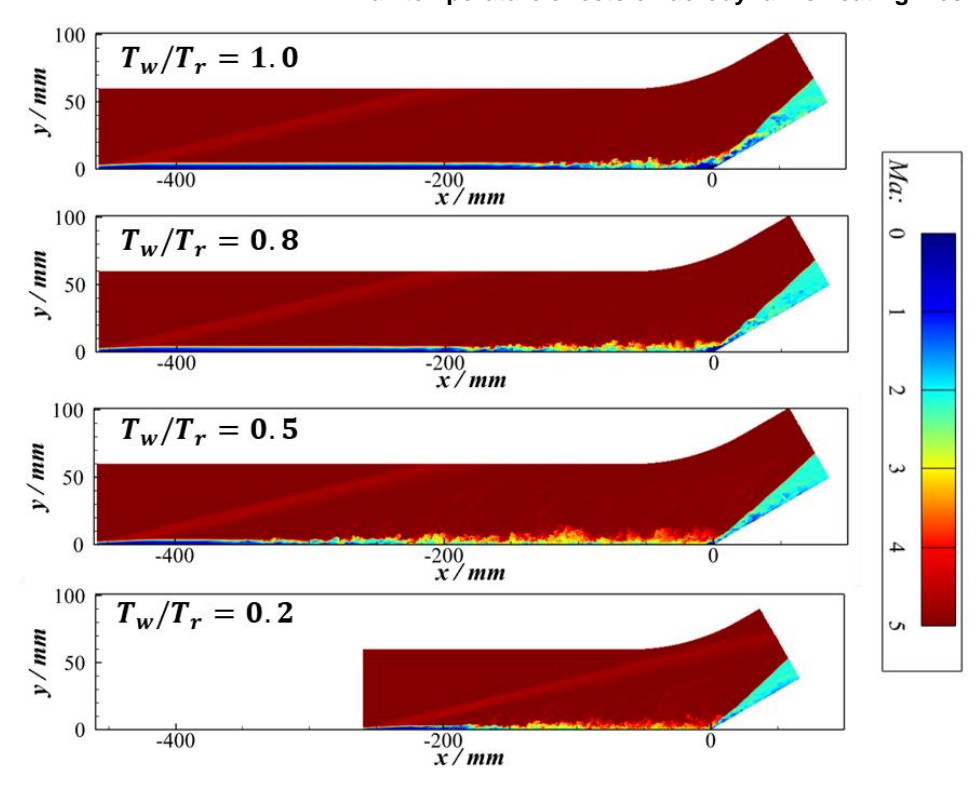


Fig. 7 Transition process of turbulent boundary layer and instantaneous flow fields of STBLI for different wall temperatures.

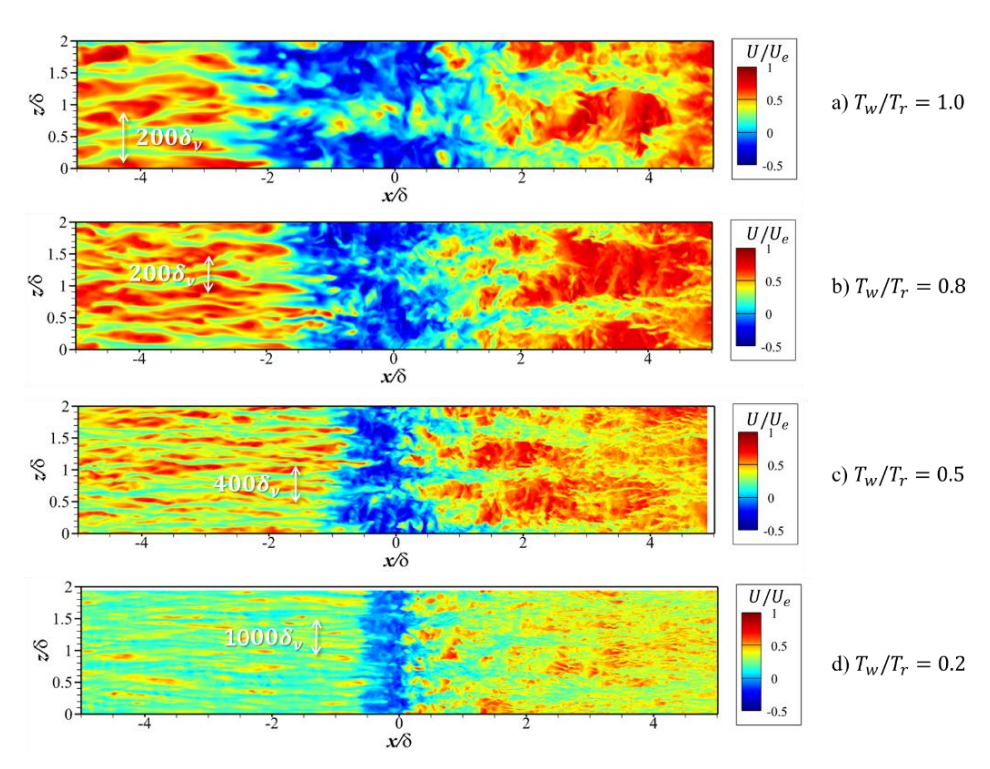


Fig. 8 Wall temperature effects on high-speed velocity streaks in near-wall viscous sublayer. The slice heights $y^+ = 10$ for all cases.

The turbulent results have been averaged over time and spanwise direction and the average flow fields are provided in Fig. 9. The results show that wall temperatures have little effects on the mainstream shock wave but great effects on the separation bubbles around the corner. As the wall temperature increases, the shock feet around the corner become more curved. The average separation bubbles of the 4 cases are extracted from the flow field for comparison in Fig. 9(e). The bubbles both are flat and close to triangle shapes. As the wall temperature decreases, the bubble

shrinks and the recirculation center moves toward the wall.

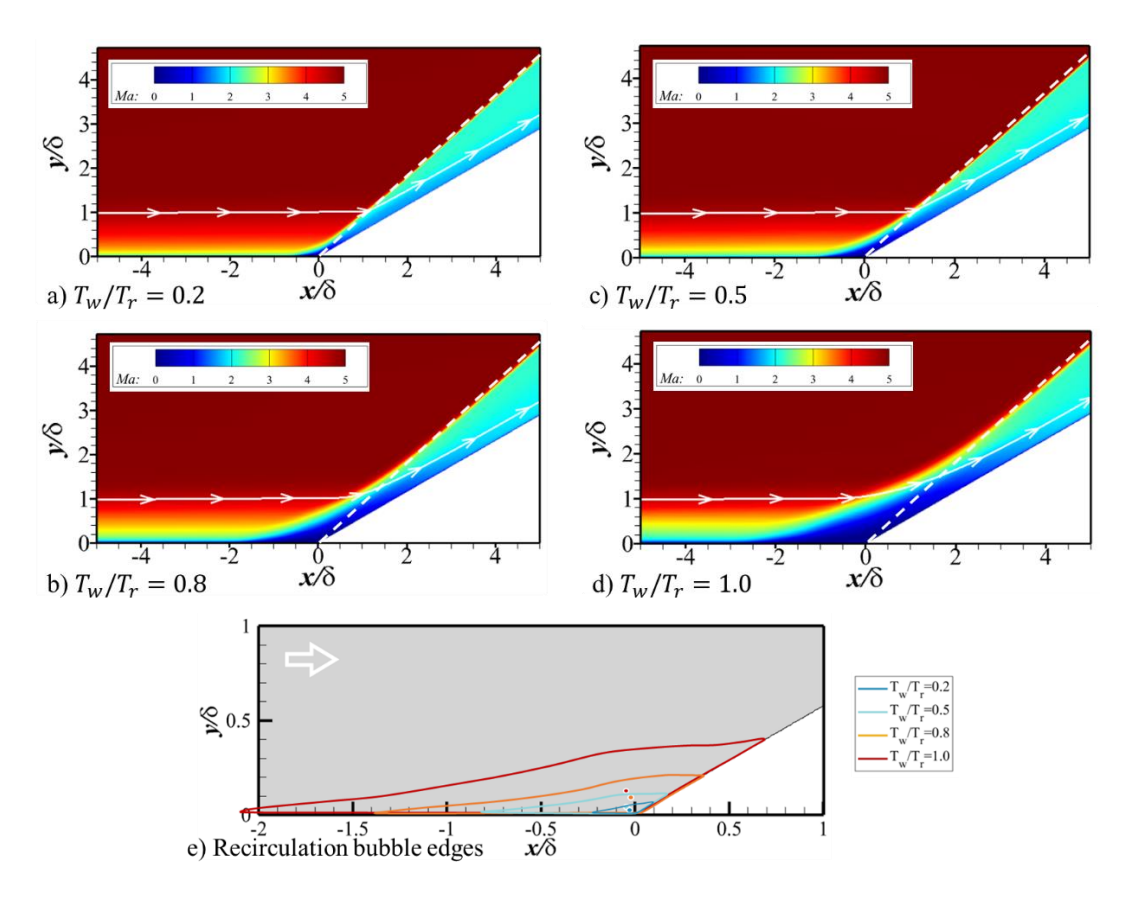


Fig. 9 (a) \sim (d) Wall temperature effects on the average flow fields and (e) recirculation bubbles. The white dash lines represent theoretical shock and the streamlines represent boundary layer edges in (a) \sim (d). The corresponding points represent the recirculation center in (e).

According to the skin friction distribution, the separation lengths are further obtained for different wall temperatures and power fitting results are provided as shown in Fig. 10. In upstream undisturbed turbulent boundary layer, the skin friction coefficients decrease slowly for all cases and the case T02 gives the maximum skin friction coefficient. Around the corner, the skin friction decreases dramatically and go below zero, which indicates the occurrence of separations. Downstream of the corner, the skin friction increases with the recovery of the boundary layers and go above zero, which indicates the reattachment. Coincidentally, all cases recover to the same peak downstream. The separation lengths are further obtained and fitted by linear law proposed by Spaid et al. [27] and power law of 0.85 proposed by Zhu et al. [2] as shown in Fig. 10(b). The results show that the linear fitting is a simple but acceptable approximation, which is expressed as the following formula:

$$\frac{L_{sep}}{\delta} = 2.9(\frac{T_w}{T_r} - 0.08). \tag{2}$$

However, the theory of Zhu et al. [2] deviates from the present results, which infer that the exponent is 0.85. The present power fitting gives that:

$$\frac{L_{sep}}{\delta} = 2.8 \left(\frac{T_w}{T_r}\right)^{1.45} \tag{3}$$

There is an essential difference between the exponent above 1 and below 1. The deviation of Zhu's power theory [2] may be attributed to their neglect to consider the extreme cold wall condition for which the separation length will shrink more slowly, resulting in an exponent greater than 1.

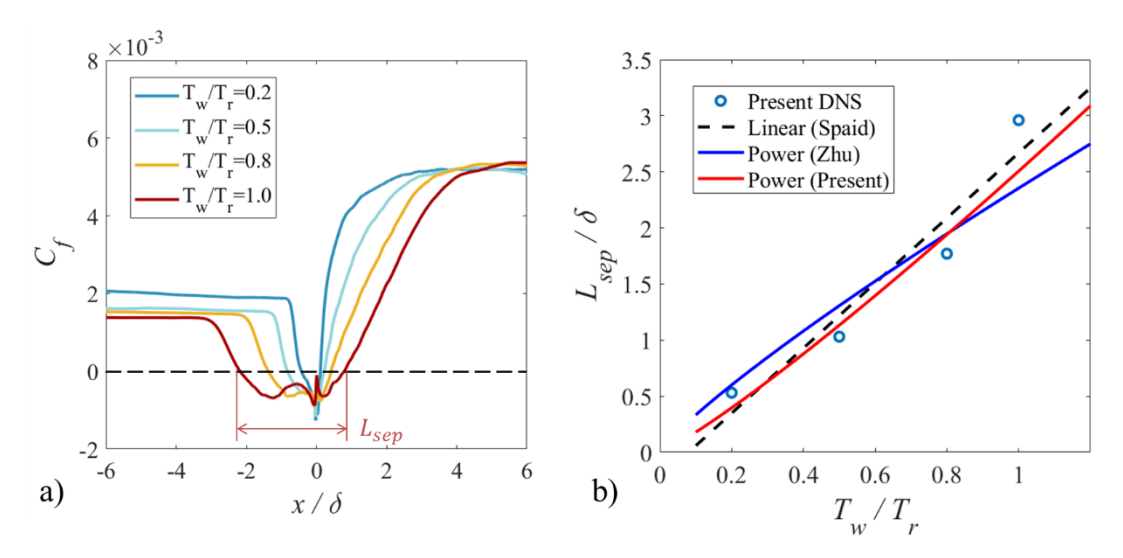


Fig. 10 (a) Friction coefficient distribution and (b) quantitative fitting of the separation lengths for different wall temperatures.

According to the wall pressure distribution, the upstream interaction lengths are investigated for different wall temperatures. As shown in Fig. 11, the wall pressure ratio increases more sharply for lower wall temperature but all basically reach the inviscid theoretical value downstream of the corner. An interesting point is that all the pressure rise curves for different wall temperatures pass through the same point near the corner vertex as shown in Fig.11. According to Chapman's free interaction theory [28], the upstream pressure rise is not affected by the downstream and the platform pressures are predicted to be about 3.55~3.76 for present wall temperature conditions, which is close to the pressure ratio at the intersection point. Furthermore, the interaction scales, which are defined as the distance between the initial rise points of the wall pressure and the vertices of the compression corner, are calculated and nondimensionalized by the method of references [9]& [10]. As shown in Fig. 12, the maximum relative deviation between the results and the Souverein's correlation ($L^* =$ $1.3S_e^{*3}$) is 25%. Reference data have also been collected and presented in Fig. 12, including the adiabatic results compiled by Souverein et al. [9]and some recent non-adiabatic results from Jaunet et al.[10], Spaid & Frishett [27], Schreyer et al. [29], Bhagwandin et al. [30], Volpiani et al. [7]and Zuo et al. [8]. The results, especially non-adiabatic results, are around the fitting lines and hence basically verifies the wall-temperature-corrected theory proposed by Jaunet et al. [10].

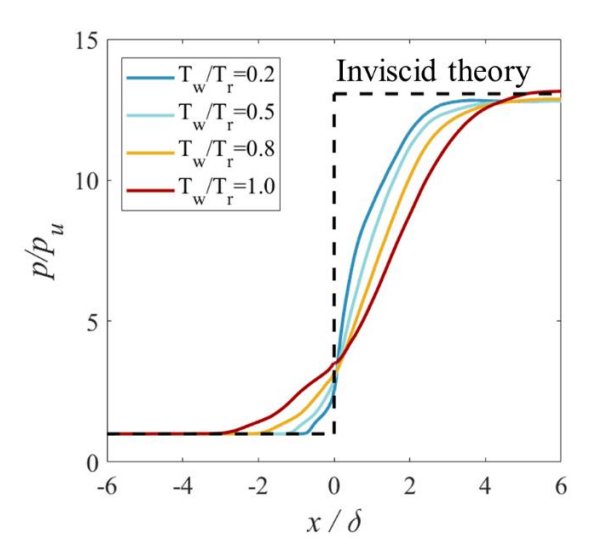


Fig.11 Wall temperature effects on wall pressure distribution. The subscript u means the value at the undisturbed reference position (x = -60 mm).

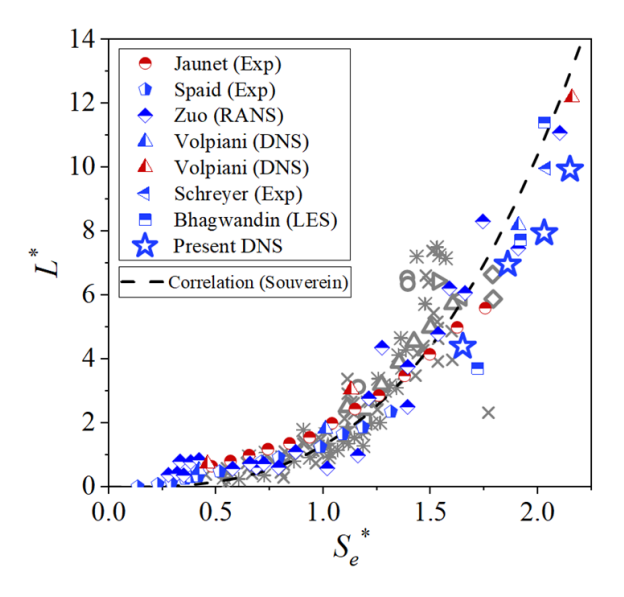


Fig. 12 Normalized interaction length compared with the scaling theory proposed by Souverein et al. [9]and corrected by Jaunet et al.[10]. The gray symbols are from Souverein et al. 2013, for adiabatic cases, the red symbols represent hot wall conditions and the blue symbols represent cold wall conditions.

Above all, cold wall temperatures lead to more coherent turbulent structures and weaken the shock surface fluctuation. Cold walls also reduce separation lengths and the present study quantitively suggests that there are limitations in Zhu et al. 's theory of 0.85 power relation [2] between separation length and wall temperature, which is incorrect for extremely cold walls, and further research is needed. Finally, the present study quantitatively validates the wall-temperature-corrected interaction scaling theory in recent literature [10].

4. Wall Temperature Effects on Aerodynamic Heating in STBLI

The instantaneous hot structures in STBLI for cold walls are investigated first and case T02 is presented in Fig. 13 as a representative example. The results show that there are irregular hot fluid masses ejecting into the mainstream at the edge of the boundary layer. The enlarged image provides more details which show that in the extreme near-wall area, the high-temperature fluid gathers at a height away from the wall and the edge of the high-temperature fluid near the wall is a relatively regular wave shape. In the interaction region, the shock angle is larger where the high-temperature fluid passes through. The extremely high-temperature fluid appears on the ramp, which is distributed at the bottom of the boundary layer and near the shock wave. These high-temperature fluid brings intense aerodynamic heating to the walls.

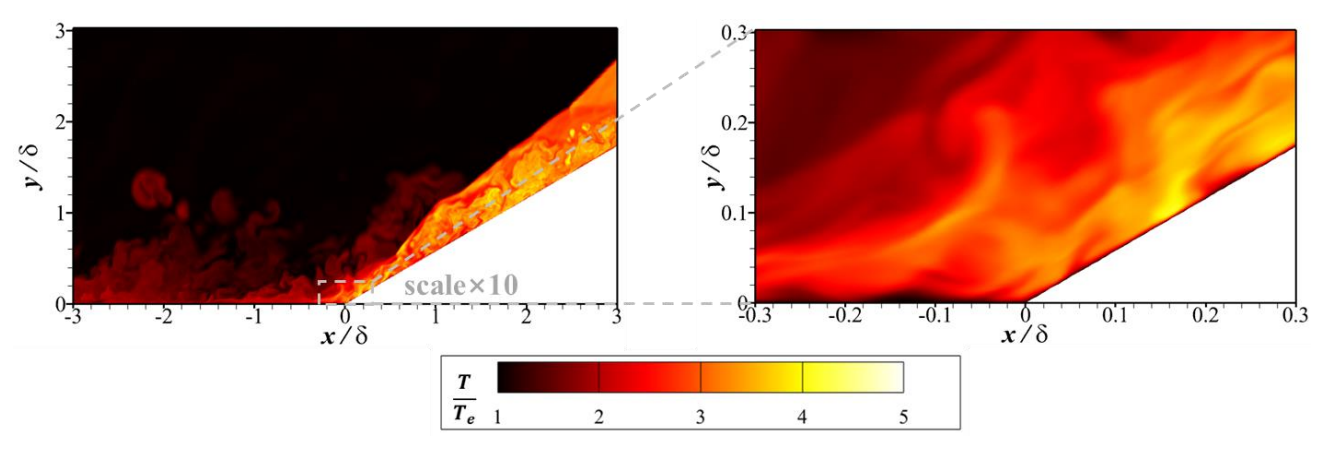


Fig. 13 Instantaneous hot structures in temperature field of STBLI for cold wall conditions, taking case T02 as an example.

The dimensionless wall heat fluxes for different wall temperatures are shown in Fig.14, which exhibit very significant wall temperature effects and complex aerodynamic heating variation during the interaction. As expected, the lower the wall temperature, the greater the wall heat flux as shown in Fig. 14(a), which can be explained by the greater driven temperature difference. However, the detailed distribution shows big differences. At x < 0, case T02 shows a notable minimum heat flux and case T08 shows a distinct two-stage heat flux increase, which can be explained by the separation bubble increase with the wall temperature increase as shown in Fig.9(e). After the reattachment points, case T02 reaches a small but sharp peak and then a plateau appears, case T05 shows a peak plateau, case T08 reaches a peak and slowly decreases, and case T10 directly and slowly decreases to negative wall heat flux. There are two interesting phenomena: one is the sharp heat flux peak for extremely cold wall; the other is the negative minimum heat flux at $x/\delta = 4$ after the peak for the adiabatic wall, which means that the local recovery temperature decreases downstream of the corner. In addition, although the cold wall increases absolute wall heat flux, it weakens the heat flux enhancement as shown in Fig. 14(b). Another interesting point is the minimum heat flux which all locate at the separation point and become notable for cold walls as shown more clearly in Fig. 14(b). Therefore, the wall temperature effects on aerodynamic heat distribution can be mainly explained by the separation bubble variation.

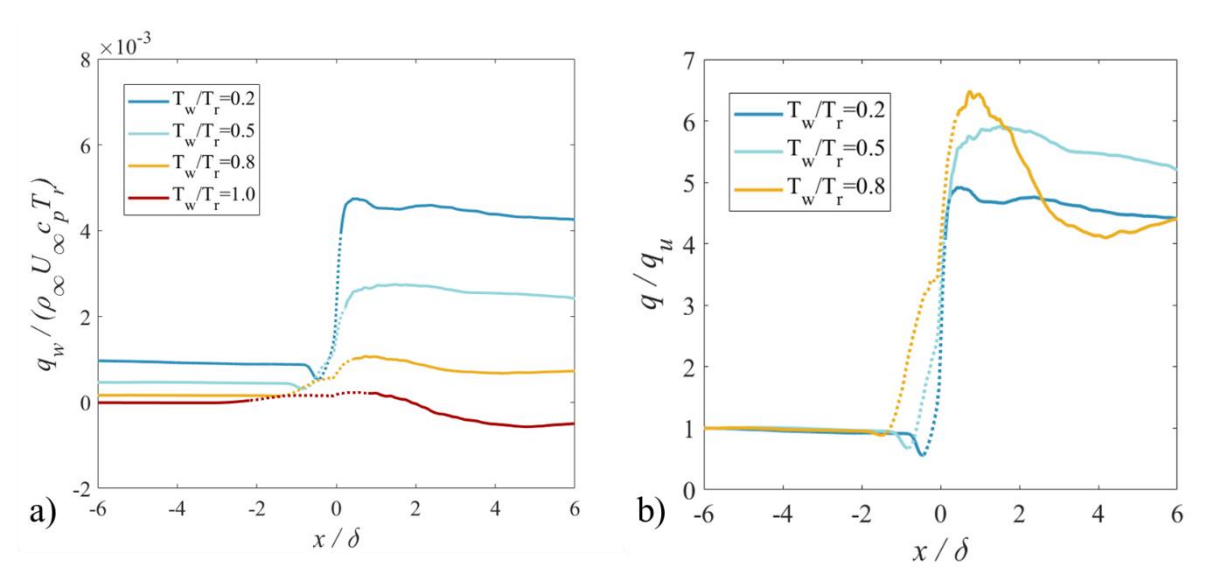


Fig. 14 Wall temperature effects on (a) dimensionless wall heat fluxes and (b) intensification heat flux ratios in STBLI. Dash lines represent the separation regions.

The mechanisms of local decrease of recovery temperature for adiabatic walls or close to the adiabatic are further investigated because it does not meet the intuitive expectation that shock waves increase the recovery temperature. The average temperature field covered by streamlines for case T10 is shown in Fig. 15(a), which shows that the temperature of near-wall fluid slightly decrease around x/δ =4 causing heat to flow into the fluid instead of the wall. For the adiabatic wall case T10, the near-wall supersonic fluid completes the turn and then accelerates exactly around x/δ =4 as shown in Fig. 15(b), which makes the fluid temperature suddenly drops. At the same time, the fluid temperature decreases to obtain energy from the near-wall and recover the total temperature so that the turbulent boundary layer can recover to equilibrium as shown in Fig. 15(c). The coupling change of the flow and temperature causes heat flux to flow to the fluid from the wall, which is the mechanism for the formation of the minimum heat flux downstream of the reattachment point. For near adiabatic case T08, there is similar process of supersonic fluid acceleration and boundary layer recovery, and the results are omitted to avoid redundancy. Above all, the acceleration of the near-wall supersonic fluid in turning process cause the heat to flow into the fluid for the "adiabatic" wall, or in other words cause the local decrease of the recovery temperature.

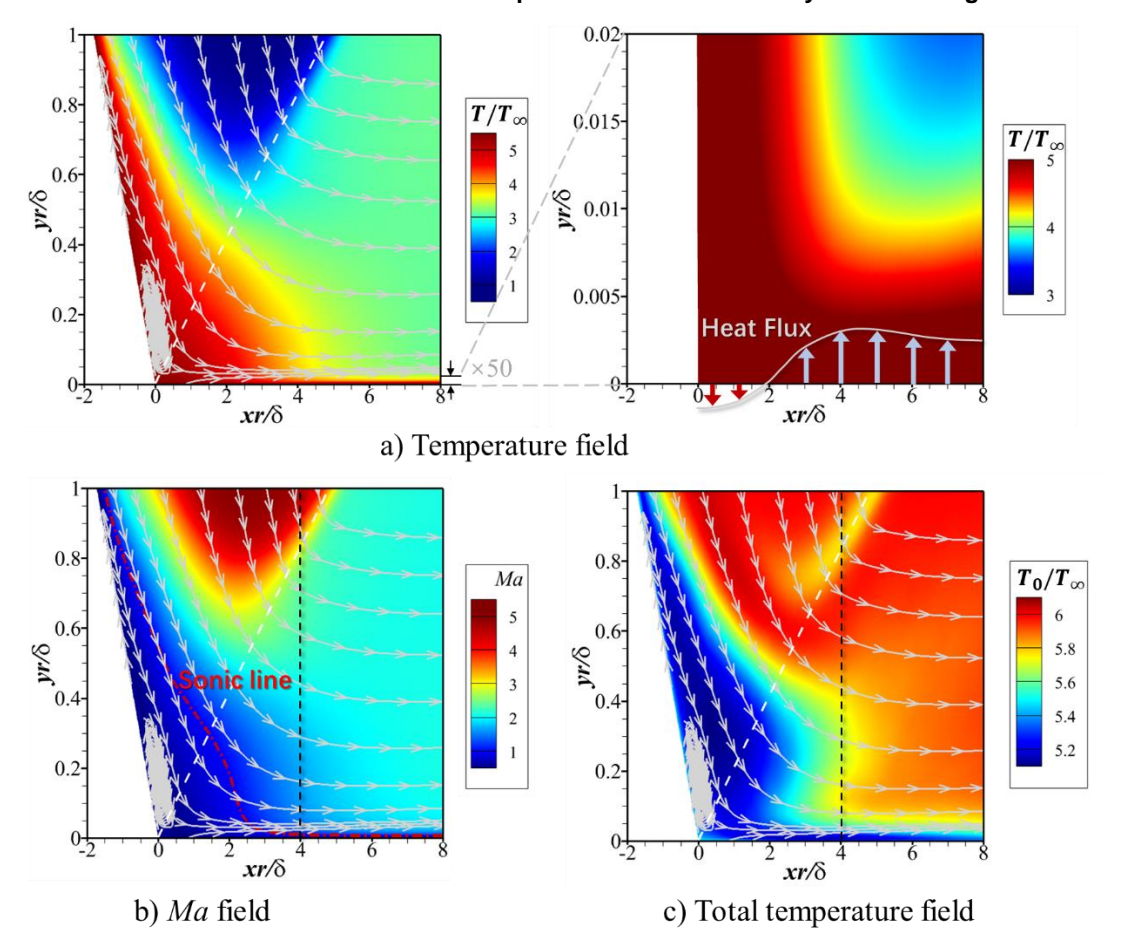


Fig. 15 Coupling analysis of temperature field and flow filed for an adiabatic wall (case T10). The domain is rotated 30 degree to make the ramp horizontal and (x_r, y_r) is the ramp coordinate. The wall heat flux reaches minimum around $x_r/\delta = 4$ which is also denoted by black dash lines in (b)&(c).

Most importantly, the mechanisms of the weakened heat flux enhancement for cold walls are further investigated to explain the wall temperature effects on the aerodynamic heating peak in STBLI. Previous study of Bernardini et al. [6]found that the temperature effects on the wall heat flux enhancement in STBLI is dominated by wall pressure fluctuation enhancement, which is also proved by the present study as shown in Fig.16. The pressure fluctuation results show that the fluctuation enhancement decrease for the cold wall leading to lower enhancement of the wall heat flux ratio. Furthermore, the present analysis suggests that the more fundamental mechanisms for the wall temperature effects lie in the variation of turbulent aerodynamic heat dissipation near the wall because it reflect aerodynamic heat generation. The definition of aerodynamic heat dissipation is from Equation (1) where $\Phi_m = 2\mu \overline{S_{ij}^d} \overline{S_{ij}^d}$, $\Phi_t = 2\mu \overline{S_{ij}^d} \overline{S_{ij}^d}$. Ratios of near-wall turbulent dissipation to mean flow dissipation are provided in Fig. 17(a), indicating that turbulent aerodynamic heat dissipation dominates the aerodynamic heat generation in STBLI comparing with the ratio of 0.25 in upstream undisturbed boundary layer. The ratios all show a peak around the attachment points, which is because that the average shear around the reattachment is close to zero while the turbulent shear is enhanced due to separation bubble instability. Moreover, the higher the wall temperature, the wider the region dominated by the turbulent aerodynamic heat dissipation. Hence, the turbulent dissipation enhancement is further investigated as shown in Fig. 17(b). As the wall temperature decreases, turbulent heat dissipation enhances more weakly, resulting in an decrease of peak heat flux ratio peak. In addition, turbulent dissipation peak is sharper in the cold wall case T02, resulting in sharper wall heat flux peak. Therefore, the wall temperature effects on aerodynamic heat peak can be fundamentally explained by the near-wall turbulent aerodynamic heat dissipation enhancement.

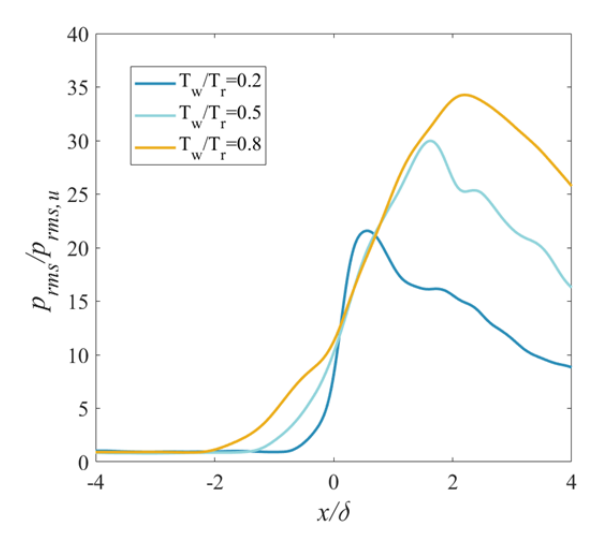


Fig. 16 Wall temperature effects on wall pressure fluctuations in STBLI.

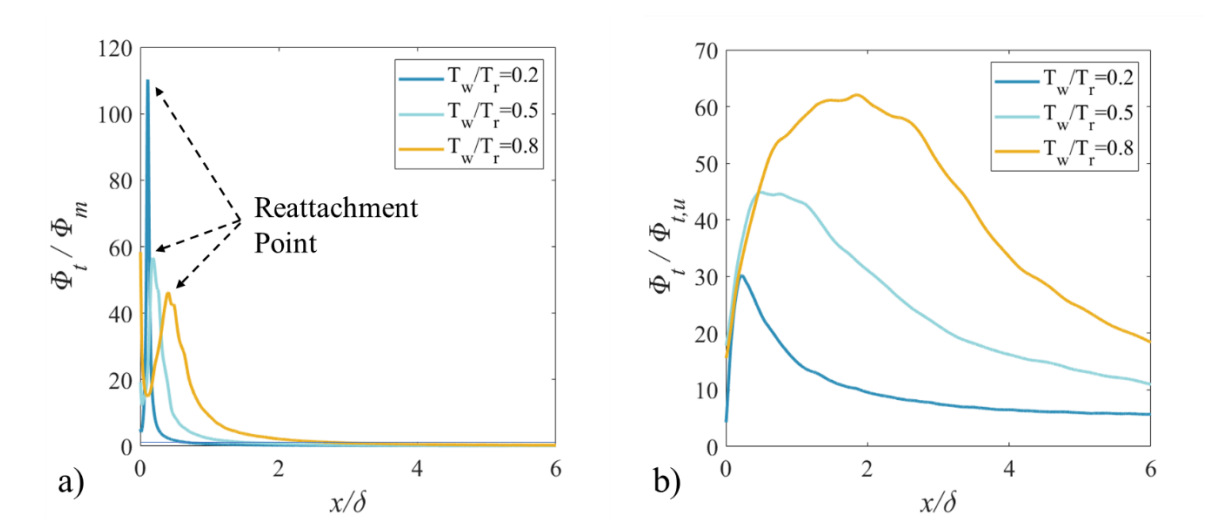


Fig. 17 (a) Ratios of turbulent dissipation to mean flow dissipation and (b) enhancement ratios of turbulent dissipation for different wall temperatures.

5. Conclusion

The paper investigates the wall temperature effects on STBLI with a focus on aerodynamic heating. The DNS method is used and validated carefully to obtain a reliable database of STBLI for different wall temperatures. The results reproduce the phenomena of the separation zone decrease for cold wall conditions and validate the non-adiabatic interaction scaling theory in the literature.

The heat transfer results show that for all wall temperature conditions there exists a peak heat flux downstream of the reattachment point, but the wall temperature greatly influences the heat flux distribution and peak values. The wall temperature effects on aerodynamic heat distribution can be mainly explained by the separation bubble variation and turning fluid acceleration. A distinct two-stage heat flux increase is observed for the hot wall, which corresponds to the expanded separation bubble. The local decrease of the recovery temperature is observed after the shock, which causes the negative heat flux minimum for near "adiabatic" wall conditions. Further analysis reveals that the underlying mechanism is the acceleration of the near-wall supersonic fluid in turning process. The wall temperature effects on aerodynamic heat peak can be fundamentally explained by the near-wall turbulent aerodynamic heat dissipation enhancement. The decrease of wall temperature leads to the decrease of the peak heat flux enhancement because the near-wall turbulent aerodynamic heat dissipation enhancement is weakened.

The wall temperature effects on aerodynamic heating in STBLI and the influence mechanisms

discussed in the paper can provide some reference for designing ground wind tunnel experiments in future research and for developing flow and aerodynamic heat control methods by wall cooling.

Acknowledgments

The study is financially supported by Tsinghua University Initiative Scientific Research Program.

Contact Author Email Address

Xueying Li: li_xy@tsinghua.edu.cn

Copyright Statement

The authors confirm that they hold copyright on all of the original material included in this paper. The authors also confirm that they have obtained permission, from the copyright holder of any third party material included in this paper, to publish it as part of their paper. The authors confirm that they give permission for the publication and distribution of this paper as part of the ICAS proceedings or as individual off-prints from the proceedings.

References

- [1] Dolling and David, S., "Fifty Years of Shock Wave Boundary Layer Interaction Research: What Next?", AIAA Journal, Vol. 39, No. 8, 2001, pp.1517-1531.
- [2] Zhu, X.-K., Yu, C.-P., Tong, F.-L. and et al., "Numerical Study on Wall Temperature Effects on Shock Wave/Turbulent Boundary-Layer Interaction", AIAA Journal, Vol. 55, No. 1,, 2017, pp. 1-10.
- [3] Delery, J. M., "Shock wave/turbulent boundary layer interaction and its control", Progress in Aerospace Sciences, Vol. 22, No. 4, 1985, pp. 209-280.
- [4] Spaid, F. W. and John, C. F., "Incipient separation of a supersonic, turbulent boundary layer, including effects of heat transfer", AIAA Journal, Vol. 10, No. 7, 1972, pp. 915-922.
- [5] Back, L. H. and Robert, F. C., "Shock wave/turbulent boundary-layer interactions with and without surface cooling", AIAA Journal, Vol. 14, No. 4, 1976, pp. 526-532.
- [6] Bernardini, M., Asproulias, I., Larsson, J., Pirozzoli, S. and Grasso, F., "Heat Transfer and Wall Temperature Effects in Shock Wave Turbulent Boundary Layer Interactions", Physical Review Fluids, Vol. 1, 2016, 084403.
- [7] Volpiani, Pedro S., Bernardini, M. and Larsson, J., "Effects of a nonadiabatic wall on hypersonic shock/boundary-layer interactions", Physical Review Fluids, Vol. 5, No. 1, 2020, 014602.
- [8] Zuo, F.-Y., Wei, J.-R, Hu, S.-L. and et al., "Effects of wall temperature on hypersonic impinging shock-wave/turbulent-boundary-layer interactions", AIAA Journal, Vol. 60, No. 9, 2022, pp. 5109-5122.
- [9] Souverein, L., Bakker, P. and Dupont, P., "A scaling analysis for turbulent shock-wave/boundary-layer interactions". Journal of Fluid Mechanics, Vol. 714, No. 1, 2013, pp. 505-535.
- [10] Jaunet, V., Debieve, J. F. and P. Dupont, "Length scales and time scales of a heated shock-wave/boundary-layer interaction", AIAA Journal, Vol. 52, No. 11, 2014, pp. 2524-2532.
- [11]Tong, F., Tang, Z., Yu, C., Zhu, X. and Li, X., "Numerical analysis of shock wave and supersonic turbulent boundary interaction between adiabatic and cold walls", Journal of Turbulence, Vol. 18, No. 6, 2017, pp. 569-588.
- [12]Zhu, K., Jiang, L. X., Liu, W. D., Sun, M. B., Wang, Q. C., and Hu, Z. W. "Wall temperature effects on shock wave / turbulent boundary layer interaction via direct numerical simulation", Acta Astronautica, Vol. 178, 2021, 499-510.
- [13]Fu D., Ma Y., Li X. and et al., Direct Numerical Simulation of Compressible Turbulence, Science Press, 2010. (in Chinese)
- [14] Duan L., Beekman I. and Martin M. P., "Direct Numerical Simulation of Hypersonic Turbulent Boundary Layers. Part 2. Effect of Wall Temperature", J. Fluid Mech., Vol. 655, 2010, pp.419-445.
- [15]Pirozzoli, S., Grasso, F., and Gatski, T. B., "Direct numerical simulation and analysis of a spatially evolving supersonic turbulent boundary layer at M= 2.25", Physics of fluids, Vol. 16, No. 3, 2004, pp. 530-545.
- [16]Tong F., Yuan X., Lai J. and et al., "Wall Heat Flux in a Supersonic Shock Wave/Turbulent Boundary Layer Interaction", Physics of Fluids, Vol. 34, No .6, 2022, 65104.
- [17]Tong F., Duan J. and Li X., "Shock wave and turbulent boundary layer interaction in a double compression ramp", Computers & Fluids, Vol. 229, 2021, 105087.
- [18]Li X., Fu D., Ma Y. and et al.., "Direct Numerical Simulation of Shock Wave Turbulent Boundary Layer Interaction", Scientia Sinica, Vol. 40, 2010, pp.791-799. (in Chinese)

Wall temperature effects on aerodynamic heating mechanisms in STBLI

- [19]Ma C. & Liu J., "Effect of grid strategy on numerical simulation results of aerothermal heating loads over hypersonic blunt bodies", Acta Aeronautica et Astronautica Sinica, Vol. 44, No. 05, 2023, pp. 73–86.
- [20]van Driest, E. R., "Turbulent boundary layer in compressible fluids", Journal of the Aeronautical Sciences, Vol. 18, 1951, pp.145~160.
- [21]Trettel, A., and Larsson, J., "Mean velocity scaling for compressible wall turbulence with heat transfer", Physics of Fluids, Vol. 28, No. 2, 2016, 026102.
- [22] Walz, A., Boundary Layers of Flow and Temperature, MIT Press, 1969.
- [23]Zhang Y., Bi W., Hussain F. & She Z. "A generalized Reynolds analogy for compressible wall-bounded turbulent flows", Journal of Fluid Mechanics, Vol. 739, 2014, pp. 392–420.
- [24] Simeonides G, Haase W. "Experimental and computational investigations of hypersonic flow about compression ramps", Journal of Fluid Mechanics, Vol. 283, 1995, pp. 17-42.
- [25]De Luca L, Cardone G., Aymer De La, Chevalerie D., et al., "Goertler instability of a hypersonic boundary layer", Experiments in Fluids, Vol. 16, 1993, pp. 10-16.
- [26] Navarro-Martinez S., Tutty O. R., "Numerical simulation of Görtler vortices in hypersonic compression ramps", Computers & Fluids, Vol. 34, No. 2, 2005, pp. 225-247.
- [27] Spaid, F. W. & Frishett, J. C, "Incipient separation of a supersonic, turbulent boundary layer, including effect of heat transfer", AIAA Journal, Vol. 10, No. 7, 1972, pp. 915–922.
- [28] Chapman, D. R., Kuhen, D. M. and Larson, H. K. "Investigation on separated flows in supersonic and subsonic streams with emphasis on the effect of transition". NACA TN 3869, 1957.
- [29]Schreyer A. M., Sahoo D., Williams O. J. H. & Smits A. J., "Experimental investigation of two hypersonic shock/turbulent boundary-layer interactions", AIAA Journal, Vol. 56, No. 12, 2018, pp. 4830–4844.
- [30]Bhagwandin V. A., Helm C. M. & Martin P., "Shock wave-turbulent boundary layer interactions in separated compression corners at Mach 10", AIAA Scitech 2019 Forum, 2019, p. 1129.